Full Paper

and Polymers

Effect of Particle Size on Silver Nanoparticle Deposition onto Dielectric Barrier Discharge (DBD) Plasma Functionalized Polyamide Fabric

Nguyen Khanh Vu,[†] Andrea Zille,[†] Fernando Ribeiro Oliveira,
Noémia Carneiro, Antonio Pedro Souto*

The effect on the deposition of three different size silver nanoparticles (AgNPs) onto a polyamide 6,6 (PA) fabric pre-treated using air dielectric barrier discharge (DBD) plasma was investigated. The SEM, EDS, and XPS analysis confirm that the smaller is the diameter of AgNPs, the higher the amount of adsorbed NPs on the PA. The DBD treatment on PA induces a threefold increase in Ag adsorption. The result confirms a dual effect on the wettability of the plasma treated PA substrate. AgNPs slightly enhance hydrophobicity of the PA surface and, at the same time, protect it against the plasma aging effect.
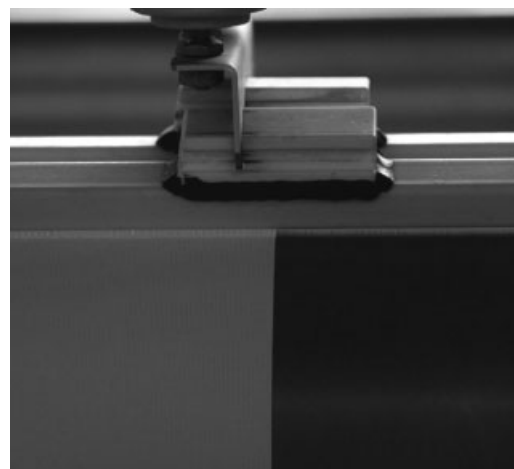
1. Introduction

Currently, nanotechnology is considered the most promising technology for commercial applications in the textile industry.[1] Nanotechnology can provide high functional durability for fabrics due to nanoparticles extremely large surface area and high surface energy, without affecting their breathability or hand feel.[2–4] In the last several years, nanotechnology has renewed the interest for finishing of textiles.[5,6] A wide range of antimicrobial agents has been employed to limit the easy propagation of microorganisms in textile materials.[7,8] Among them, different types of nanomaterials like copper, zinc, titanium, magnesium, gold, alginate, and silver have been employed but silver nanoparticles have proved to be the most effective.[9] Silver nanoparticles shows higher efficient antimicrobial prop-

erty compared to silver salts due to their extremely large surface area, which provides better contact with microorganisms.[10] Moreover, silver ions exhibits low toxicity and have a far lower propensity than classic antibiotics, to induce high-level, single-step resistance mutations.[11] Different textile materials have been functionalized with silver nanoparticles.[12–14] However, the most of these materials are based on synthetic fibres, which are often highly hydrophobic. Higher hydrophilicity and improved adhesive properties of hydrophobic fibres can be obtained by plasma functionalization and etching. In particular, non-thermal plasmas are particularly suited because most textile materials are heat sensitive polymers.[15–17] Atmospheric plasma is an alternative and cost-competitive method to wet chemical treatments, avoiding the need of expensive vacuum equipment and allowing continuous and uniform processing of fibres surfaces.[18] Several atmospheric plasma pre-treatments of textiles loading silver nanoparticles have been widely reported in litera-

N. K. Vu, Dr. A. Zille, F. R. Oliveira, Prof. N. Carneiro, Prof. A. P. Souto
Department of Textile Engineering, University of Minho, Campus de Azurém, 4800-058 Guimarães, Portugal
E-mail: souto@det.uminho.pt
[†]These authors contributed equally to this work.

ture.[19–22] Among them the dielectric barrier discharge technology (DBD) is one of the most effective non-thermal plasma sources[23] and has been attracting increasing interest for industrial applications.[24,25]

The purpose of this paper is to study the silver nanoparticle size effects on the deposition onto polyamide fabrics after surface chemical modification and activation by air DBD plasma pre-treatment. Polyamide fibres is one of the most important synthetic fibres used in textile industry due to its excellent mechanical, thermal and chemical properties and its silver surface functionalization by atmospheric plasma has been broadly investigated especially that concerning the antimicrobial activity.[13,20,22,26–28] The size-dependent antimicrobial activity of silver nanoparticles has already been investigated concluding that the smaller the nanoparticle, the more it releases Ag^+ ions and the higher the antibacterial effect.[29–31] However, there are not reports on the size-dependent physical and chemical surface effects of the deposited nanoparticle on DBD plasma functionalized polyamide (e.g. electrostatic chemical interactions, wettability and plasma aging). Three different in size silver nanoparticles have been employed, two commercials (10 and 20 nm) and one synthetized in our laboratory (∼50 nm). Dynamic light scattering and spectroscopic techniques have been used to characterize nanoparticles. Scanning electron microscope (SEM), contact angle measurements and X-ray photoelectron spectroscopy (XPS) have been used to study the changes of surface morphology, wettability and chemical composition of the plasma-treated polyamide fabrics with and without loaded silver nanoparticles (AgNPs).

2. Experimental Section

2.1. Materials

Commercial polyamide 6,6 (PA) fabric with a warp density of 40 threads $\cdot$ cm^{-1}, a weft density of 18 threads $\cdot$ cm^{-1} and a surface density of 135 g $\cdot$ m^{-2} was used in this study. The samples were pre-washed with a solution of 1% non-ionic detergent at 30 °C for 30 min and then rinsed with water for another 15 min, before DBD plasma treatment in order to minimize contaminations. All reagents were analytical grade purchased from Sigma–Aldrich, St. Louis, MO, USA and used without further purification.

2.2. Plasma Treatment

The DBD plasma treatment was conducted in a semi-industrial prototype machine (Softal Electronics GmbH/University of Minho) working at room temperature and atmospheric pressure, using a system of metal electrode coated with ceramic and counter electrodes coated with silicon with 50 cm effective width, gap distance fixed at 3 mm and producing the discharge at high voltage 10 kV and low frequency 40 kHz. The discharge power supplied by the electrodes and the speed may be varied, with maximum

discharge of 1.5 kW and speed of 60 m $\cdot$ min^{-1}. Five different dosages (0.5, 1, 2, 2.5 and 3.5 kW $\cdot$ min $\cdot$ m^{-2}) were tested in order to optimize the plasmatic effect onto the PA surface. The machine was operated at the optimized parameters: 1 kW of power, velocity of 4 m $\cdot$ min^{-1}, 5 passages corresponding to a dosage of 2.5 kW $\cdot$ min $\cdot$ m^{-2}. Plasmatic dosage was defined by the Equation (1):

$$\text{Dosage} = \frac{NP}{vl} \tag{1}$$

where, N = number of passages, P = power (W), v = velocity (m $\cdot$ min^{-1}) and l = width of treatment (0.5 m).

2.3. Silver Nanoparticles

Three types of silver nanoparticles (AgNPs) were used. Two commercially available AgNPs of 10 and 20 nm with a concentration of 0.02 g $\cdot$ L^{-1} dispersed in aqueous buffer, containing sodium citrate as stabilizer, were provided by Sigma–Aldrich, St. Louis, MO, USA. AgNPs colloidal dispersion with a concentration of 0.02 g $\cdot$ L^{-1} was synthetized in laboratory by a modified stepwise method of the conventional reduction technique described by Lee and Meisel,[32] in order to improve the synthesis of spherical and size controlled nanoparticles. During the process the dispersion was mixed vigorously. All solutions of reacting materials were prepared in distilled water. A 100 ml of 1 mM silver nitrate ($AgNO_3$) was heated to boiling in a 250 ml flask. To this solution 10 ml of 1% trisodium citrate ($Na_3C_6H_5O_7$) was added drop by drop (3.8 mM final concentration). The pH value of reaction solution was adjusted by further addition of nitric acid or NaOH at pH 7.7. At the end of the citrate addition, distilled water was added to restore the initial volume. The solution was heated again to boiling temperature until colour's change is evident (pale yellow). Then it was removed from the heating element and stirred until cooled to room temperature.

2.4. Silver Nanoparticle Deposition on Polyamide Fabrics

Control and DBD plasma-treated PA fabrics (0.1 g) were immersed in 3 ml of AgNPs dispersions (10, 20 and 50 nm) under a 200 rpm orbital shaking using a sterile six-well cell culture plate for 15 min and dried at room temperature. Thereafter, all samples were cured at 100 °C for 5 min. Then the samples were rinsed with deionized water and dried at room temperature. The entire procedure was repeated twice. Two controls were used: a pristine control and a control that followed the same procedure of nanoparticle deposition as describe above but without AgNPs.

2.5. Spectrophotometric Measurements

UV–Vis absorption spectroscopy of AgNPs was recorded on a Unican UV–VIS 2 spectrophotometer. Aliquots of the dispersion were taken out at different times to evaluate the colloidal silver dispersion stability. Each sample was diluted three times before being measured in order to maintain the concentration in the linear zone. The synthetized AgNPs dispersion was diluted to obtain the

same absorbance of the commercial AgNPs which concentration is known ($0.02 \, mg \cdot L^{-1}$).

The colour reflectance of the PA fabrics untreated and plasma treated with adsorbed AgNPs were measured using a Spectraflash 600 (Datacolor) spectrophotometer with standard illuminant D65 (LAV/Spec. Excl., d/8, D65/10°) between 360 and 700 nm. All measurements were performed in triplicate. The data were expressed as the percentage of nanoparticles maximum wavelength absorbance increase with respect to the untreated and plasma treated PA controls.

2.6. Dynamic Light Scattering (DLS)

The particle size distribution (z-average-size) and the polydispersity index (PDI) of the silver nanoparticles were determined with a Zeta Sizer-Nano series Malvern Instruments. The samples were measured at a constant temperature of $25 \pm 1 °C$. The results were averaged over 30 runs. Each value was obtained by averaging measurements of three samples.

2.7. Zeta Potential Measurements

The ζ-potentials were determined in an electrophoretic light-scattering apparatus (Zeta Sizer-Nano series Malvern Instruments) to examine nanoparticle colloidal stability and charge. The electrophoretic determinations of ζ-potentials were made in aqueous media at moderate electrolyte concentration. Each value was obtained by averaging measurements of three samples.

2.8. Contact Angle Measurement

The water surface wettability of PA fabrics treated and untreated with plasma with and without silver nanoparticles were characterized with Dataphysics equipment using OCA20 software with video system to capture images in static and dynamic modes. All the measures were performed 14 days after the plasmatic treatment and AgNPs deposition in order to evaluate the aging effect.

2.9. Energy Dispersive Spectroscopy (EDS) and X-Ray Photoelectron Spectroscopy (XPS)

Chemical analyses of samples were performed with EDS and XPS techniques. EDS used an EDAX Si(Li) detector and an acceleration voltage of 5 kV. XPS measurements were performed on aVG Scientific ESCALAB 200A equipment with PISCES software for data acquisition and analysis. For analysis, an achromatic Al (Ka) X-ray source operating at 15 kV (300 W) was used, and the spectrometer, calibrated with reference to Ag 3d5/2 (368.27 eV), was operated in CAE mode with 20 eV pass energy. Data acquisition was performed with a pressure lower them $1 \, E^{-6} \cdot Pa^{-1}$. Deconvolution into sub-peaks was performed by least-squares peak analysis software, XPSPEAK version 4.1, using the Gaussian/Lorenzian sum function and Shirley-type background subtraction (or linear consideration of the data).

2.10. Scanning Electron Microscopy (SEM) and Scanning Transmission Electron Microscopy (STEM)

Morphological analyses of AgNPs and PA samples were carried out with an Ultra-high resolution Field Emission Gun Scanning Electron Microscopy (FEG-SEM), NOVA 200 Nano SEM, FEI Company. Secondary electron images were performed with an acceleration voltage between 5 and 10 kV. Backscattering Electron Images were realized with an acceleration voltage of 15 kV. Samples were covered with a film of Au-Pd (80 20 wt.-%) in a high-resolution sputter coater, 208HR Cressington Company, coupled to a MTM-20 Cressington High Resolution Thickness Controller. For STEM nanoparticle analysis, the synthetized silver colloid suspension was dropped in copper grids with carbon film 400 meshes, 3 mm diameter. The average size was extrapolated measuring the average diameter based in 50 observations.

3. Results and Discussion

3.1. Nanoparticle Synthesis and Characterization

The size distribution of colloidal dispersion of solid particles is determined by the ratio between the rates of nucleation of the solid cores, their subsequent growth, and aggregation. As the initial concentrations of reagents ($AgNO_3$ and sodium citrate) are high, a large number of nuclei are quickly generated, consuming a major fraction of the metal species in the system and resulting in the formation of small nanoparticles with relatively uniform size distribution.[33] However, in general, a wide distribution of particle size and shapes, from spheres and cubes to rods and needles, is a typical feature of silver colloids prepared by citrate reduction.[34–36] STEM and SEM data (Figure 1) show that the method used in this work is a simple strategy for control over the shape of the nanoparticles obtaining spherical-like nanoparticle with an average size of 50 nm ($\pm 27\%$; $N = 50$). The method includes a rapid drop in temperature at the end of the nucleation stage when the dispersion started to become slightly coloured and a weak absorption peak at around 400 nm appeared. When the dispersion started to boil again, the absorption peak shifted gradually from 400 to 430 nm, accompanied by the continuous increase in the absorbance intensity, meaning the continuous growth of the silver nanoparticles. It is known that the low reaction temperature in the growth phase is helpful to control the nanoparticle size, size distribution and shape that are determined by both processes of nucleation and growth, which are greatly affected by reaction temperature.[37,38]

UV–Vis absorption spectra of Ag colloidal particles could provide information about the particle concentration (absorbance), particle size (position of λ_{max}), and dispersity of particle size in solution (width of absorbance band). The average sizes of commercial silver colloids are 10 and 20 nm, corresponding to intense and narrow UV–Vis maximum absorption peaks (λ_{max}) at 395 and 404 nm, respectively
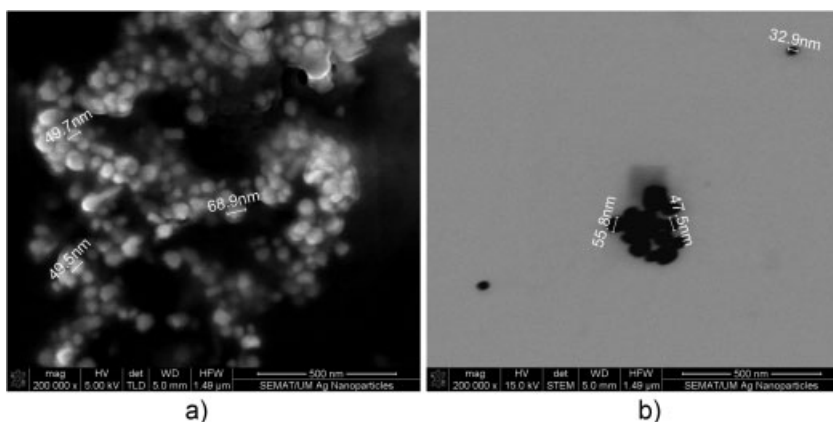
Figure 1. SEM (a) and STEM (b) images (×200 000 magnification) showing spherical-like silver nanoparticles on the order of 50 nm in diameter (± 27%; $N=50$).
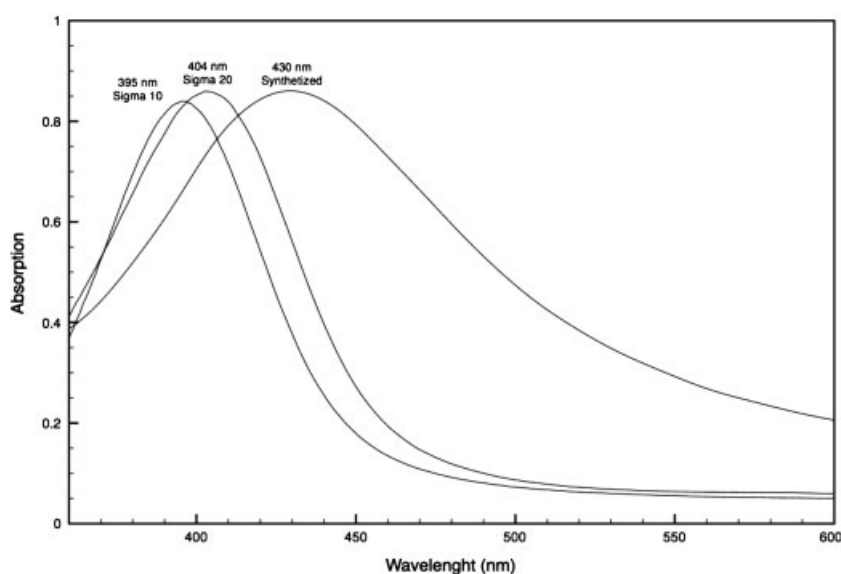

Figure 2. UV–visible spectra of the commercial (Sigma 10 and 20) and synthetized silver nanoparticles and their respective maximum peaks of absorption. Commercial samples were diluted 3 times before recording the spectra. The synthetized nanoparticles were diluted at the same absorption of the commercial ones.

Indeed, the spectrum of the synthetic silver colloid, with an average size of 50 nm, is typical of those for hydrosols of AgNPs prepared by reduction with sodium citrate and is characterized by an asymmetric absorption band with maxima at 430 nm with a large tail that extends into the red.[44–47] The broader width of the synthetized nanoparticle spectra supports the higher polydispersity of these nanoparticles. Broader bands at high wavelength also result usually in the appearance of a high level of aggregation.[48] Therefore, to monitor the stability of the synthetized silver colloid, we have measured the absorption, size distribution and polydispersity of the colloid after different periods of time. The absence of significant differences in absorbance peak, z-average-size and polydispersity after 3 weeks indicates that the nanoparticles do not aggregate (data not shown).

The nanoparticle size distribution (z-average-size) and the PDI of the commercial and synthetized AgNPs were also confirmed by dynamic light scattering (Table 1). The measured z-average and PDI ($\sim$0.2) of the commercial nanoparticles show that these NPs are very monodisperse confirming the data provided by the producer and the UV–Vis spectra of the surface plasmon resonance. The z-average (53.34 ± 16.81) and the PDI ($\sim$0.3) values of the synthetized silver NPs are consistent with those obtained from the SEM/STEM and UV–Vis analysis, respectively, indicating higher polydispersity.

The surface charge of AgNPs can be evaluated by means of a measurement of the electrical potential at the interface between the moving and the stationary solvent layers around the colloidal particle. This potential is referred as zeta potential (ζ) and provides useful information about the charge carried by the nanoparticle and, therefore, about its stability and ability to interact with molecules.[49] Generally, a suspension that exhibits a ζ potential less than ±20 mV is considered unstable and will result in particles settling out of solution in the absence of other factors.[50] As seen from Table 1, all the used silver nanoparticles possess a high negative zeta-potential at the working pH (7.7). High values in ζ potential indicate an increase in the surface charge and consequently higher stability of silver nano-

(Figure 2). Peaks in this region are generally observed and attributed to the surface plasma excitation of monodisperse small size silver particle. These experimental results are in good agreement with several theoretical studies that have shown a dependence of the UV absorption maximum on the size of spherical metal nanoparticles.[39–41] The general trend they found is that the absorption peak shifts towards longer wavelengths as particles become bigger.[42] The dipolar adsorption is dominant for particles smaller than 20 nm, instead above 30 nm, dipolar scattering and quadrupolar adsorption play important roles, accompanied by a significant broadening in the absorption peak.[43]

Table 1. z-Average size (nm), polydispersity index (PDI) and ζ-potential (mV) values of used nanoparticles.

Nanoparticle	Z-average size [nm]	Polydispersity Index	ζ-potential [mV]
Sigma 10	8.26 ± 2.12	0.188 ± 0.021	−27.8 ± 10.5
Sigma 20	18.55 ± 5.70	0.198 ± 0.025	−36.7 ± 12.1
Synthetized	53.34 ± 16.81	0.304 ± 0.038	−41.6 ± 10.0

Data are means ± SD ($n = 3$).

particles in the dispersion due to electric repulsion of the negative charge of the citrate ions adsorbed on the nanoparticle surface.[51] However, the commercial nanoparticles exhibits different value of ζ potential depending of their size and lower ζ values when compared to the synthetized NPs. The ζ potential of colloid particles depends on the ionic strength and dielectric constant of the medium. An increase in dielectric constant increases the effective potential of the particle at the shear plane.[52] Thus, a higher concentration of the citrate ions on the synthetized NPs could explain its charge increase as compared to commercials NPs.

3.2. Optimization and Characterization of DBD Plasma Modification on PA Fabric Surface

To enhance the interaction between hydrophilic colloidal AgNPs and hydrophobic polyamide (PA) fibres, the surface of the fabric was modified by DBD plasma. The optimal dosage of DBD plasma discharge able to modify the PA fabric surface properties was investigated measuring the static and dynamic contact angles. As depicted in Table 2 higher DBD energy plasma dosages significantly improve the surface wettability of PA fabric. At the dosage of $2.5 \, kW \cdot min \cdot m^{-2}$, the contact angle decreased to not measureable values. The dynamic contact angles confirm that further energy increases do not lead to significant

differences in the hydrophilicity of the treated PA surface (data not shown).

Plasma treatment can induce substantial morphological changes of fibre surface especially on its roughness. The rougher the surface, the larger the surface energy of material, then the better wettability and adhesion.[53] SEM images of untreated and DBD plasma treated PA fibres show that the topography of the fibre was uniformly altered after plasma treatment in the form of ripple-like structures of sub-micron size that were induced by plasma etching (Figure 3b). Energetic and highly reactive plasma species attacked the fibre surface promoting fibre ablation and inducing increase of the fibre surface roughness and hydrophilicity-dependent properties.[21] These results are in agreement with the literature on the effects achieved by DBD atmospheric pressure plasma treatment on synthetic fibres.[24,54]

XPS analyses were used to obtain the degree of chemical modification of the PA fibres. The results obtained are shown in Table 3. In the control PA treated with air DBD plasma when the carbon content on the surface of the sample decreases, the atomic concentrations of oxygen and nitrogen are observed to increase probably due to the incorporation of these atoms during the plasma reactions that results in the formation of hydroxyl and polar amide groups on the fabric surface.[22,55] Etching may provoke chain scission in groups C−H, C−O, C−N, N−H present in the PA fibre promoting the formation of reactive species

Table 2. DBD Plasma tested parameters and measured static contact angles at different energy dosages onto PA fabric.

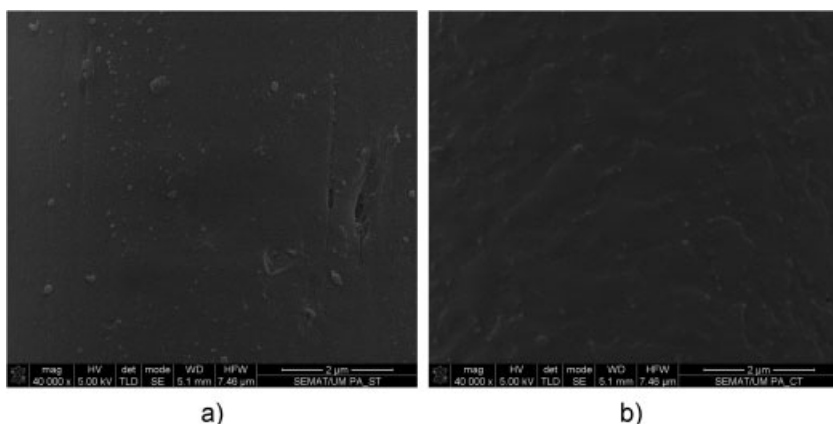| Sample	Speed [m · min⁻¹]	Number of passages	Power [kW]	Dosage [kW · min · m⁻²]	Static contact Angle [°]
Untreated	−	−	−	−	145.8 ± 6.0
1	4	1	1	0.5	90.4 ± 3.3
2	4	2	1	1	67.5 ± 2.4
3	4	4	1	2	44.4 ± 2.2
4	4	5	1	2.5	Not measureable
5	4	7	1	3.5	Not measureable

Data are means ± SD ($n = 3$).

Figure 3. SEM image of PA untreated (a) and plasma treated (b) fibres with dosage of 2.5 kW · min · m^{-2} with magnification of 40 000×.

such as O$^-$, N, N$^+$, O, OH$^-$, O$_3$, causing the decrease of carbon content and the increase of nitrogen and oxygen atoms.[26,56] The ratio N/C remained almost constant for all the samples treated under different treatment times as previously observed also for PA treated with nitrogen.[54] The increase of atomic ratio O/C after DBD plasma treatment showed higher values for XPS (∼5 nm in depth) than with EDS (∼500 nm in depth) analysis (Table 3). These results indicate a substantial incorporation of oxygen atoms only onto the fabric surface.

The analyses of C1s peaks obtained by deconvolution of the C1s core level XPS spectra of the untreated and plasma treated PA show five components (Figure 4a and b). In terms of binding energy, the peak at 284.5 eV is attributed to aliphatic carbon atoms. The peak at 285.3 eV can be associated to the amide carbonyls. The peak at 286.2 eV represents the carbon atoms neighbouring the amide nitrogen and that of at 287.6 eV is assigned to the amide carbonyl group. The peak at 288.6 eV is assigned to carboxyl groups that after plasma treatment show a significant increase (from 2.8 to 11.5%) due to the oxidation of the

methylene carbons immediately adjacent to the amide carbonyls.[25] However, the oxygen concentration in O=C−NH (from 18.4 to 15.7%) and −C=O (from 27 to 20.2%) was significantly decreased, indicating that probably more hydroxyl groups are present in the fibres. The deconvolution analysis of O1s (data not shown) confirms that after plasma treatment, the amount of oxygen singly bonded to carbon atoms, including the oxygen atoms in O=C−OH, C−C−OH, was remarkably increased.

The decrease (from 40.8 to 35.8%) in the C−C, C−H functional groups after plasma treatment is due to the aliphatic chain scission mechanisms caused by the plasma active species.[17,57] These results indicate that more polar functional groups are incorporated to PA fibres surface by the plasma treatment, enhancing the chemical–physical adsorption ability of the PA fibres.

3.3. Characterization of PA Fabrics Modified by DBD Plasma Treatment and AgNPs

The changes in fibre surface morphology, after loading the three different-sized silver nanoparticles (10, 20 and 50 nm), were evaluated by SEM. The untreated PA fabrics loaded with AgNPs (Figure 5a, c, e) are characterized by a low and irregular distribution of NPs on the fibre surface. On the contrary, the DBD treatment has positively affected the loading of silver onto the textile substrate in all the three sizes of NPs (Figure 5b, d, f). However, as previously observed by Radetic et al.,[20] at this relatively low concentration (20 ppm) the AgNPs tend to aggregate on the surface of DBD-treated PA fibres due to the thermo-migration of the nanoparticles during curing process.[58]

Energy-dispersive X-ray spectroscopy (EDS) was employed to establish the chemical identity of the observed

Table 3. Relative chemical composition and atomic ratio determined by XPS and EDS (control) of PA fabrics loaded with AgNPs, untreated and treated by DBD Plasma.

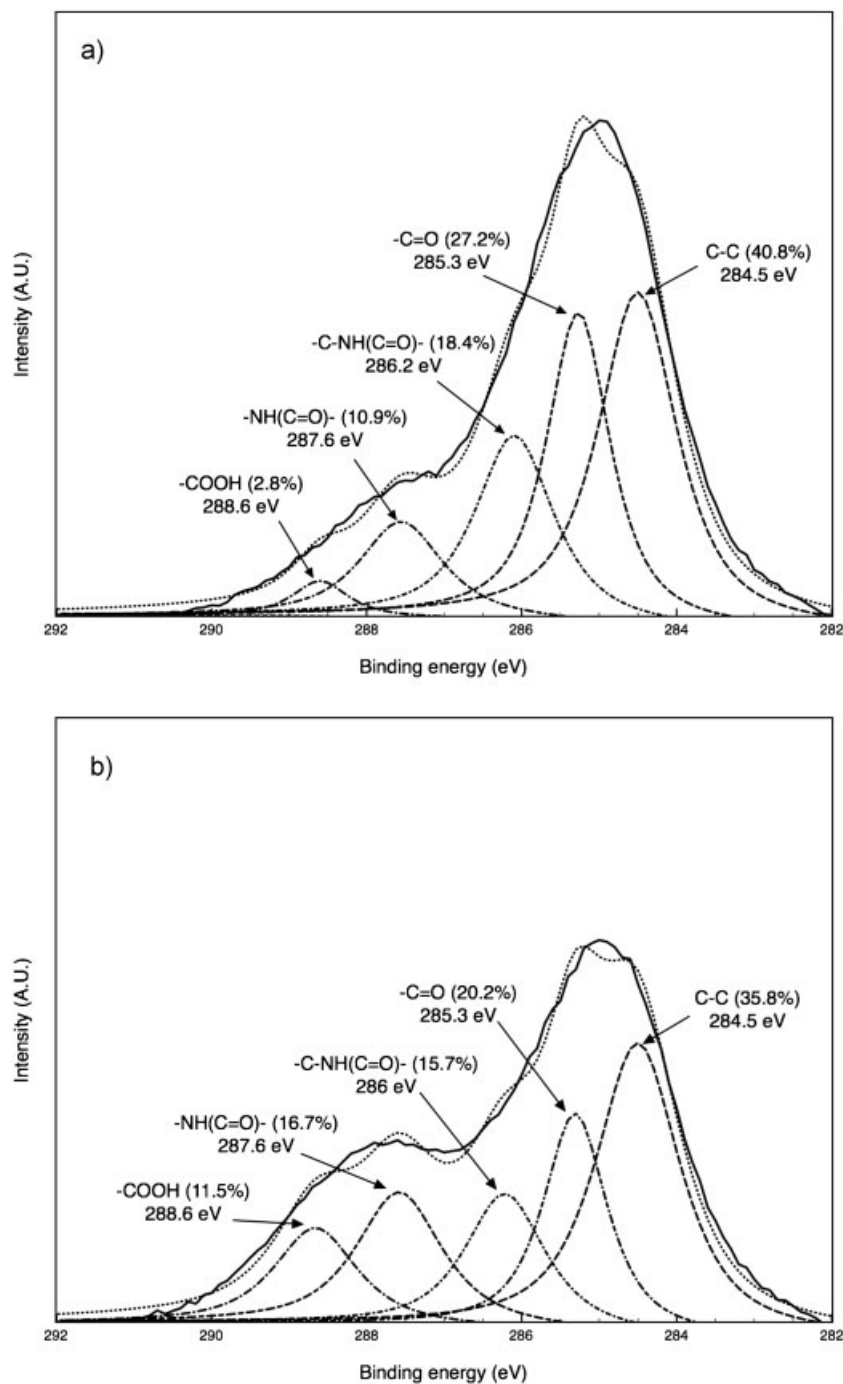| Samples	Untreated						Plasma treated					
	C At [%]	N At [%]	O At [%]	O/C ratio	N/C ratio	Ag At [%]	C At [%]	N At [%]	O At [%]	O/C ratio	N/C ratio	Ag At [%]
Control (EDS)	67.40	9.70	22.90	0.34	0.14	0	64.68	10.95	24.37	0.38	0.17	0
Control (XPS)	74.25	9.38	16.37	0.22	0.13	0	62.75	10.28	26.97	0.43	0.16	0
Sigma 10	76.02	9.38	14.54	0.19	0.12	0.06	75.89	10.08	13.80	0.18	0.13	0.23
Sigma 20	75.53	9.58	14.83	0.20	0.13	0.06	73.52	10.37	15.94	0.22	0.14	0.17
Synthetized	75.34	9.53	15.12	0.20	0.13	0.02	75.72	10.14	14.08	0.19	0.13	0.06

Figure 4. High-resolution deconvoluted XPS spectra with relative areas of the C1s binding energy region of PA fibres surface before (a) and after (b) plasma treatment.

comparison with the AgNPs loaded untreated fibres, was confirmed by X-ray photoelectron spectroscopy (XPS) and reflectance spectroscopy measures.

The XPS spectra shows that after the AgNPs loading on the plasma treated PA, independently of the particle size, the oxygen concentration returns to the same concentration of the untreated PA as the nitrogen concentration remains unaffected. This can be explained by the effect of the aging of plasma treatment accelerated by the wet treatment and thermal curing performed in this work.[59] The release of Ag$^+$ from AgNPs catalyse the production of oxygen radicals, that diffuses from the fibres to the surrounding environment leading to the observed drastic reduction of the oxygen on the PA surface.[60]

The presence of Ag in the plasma treated PA is higher for all the type of NPs than compared with the untreated PA. For a given total quantity of Ag, decreasing the size of the AgNPs leads to an increase in the specific surface area and hence to an increase of the number of NPs that can be loaded. The XPS results clearly show higher Ag peak intensity in the 10 nm NPs. This could be attributed to size-dependent higher adsorption efficiency but also to a better accessibility of the more numerous and smaller NPs. Moreover, due to the XPS limited probe depth (∼5 nm) the concentration of bigger NPs could have been underestimated. The XPS signal intensities are influenced by the Ag surface concentration as well as by the dispersion and size of the Ag on the textile surface. The exact determination of the silver surface abundance is difficult because of the variation in particle size and number (particularly for the 50 nm synthetized NPs) and of the electrostatic effects on the plasma-treated textile. However, the XPS and transmission spectroscopy analysis on the untreated fabric loaded with 10 and 20 nm AgNPs show the same XPS peak intensities and the same decrease in specular reflection. Instead, after plasma treatment, significant differences in both XPS and transmission spectroscopy could be observed. This difference cannot be explained only by the reduction of the number of nanoparticles as a function of the increase in

particles. It can be clearly seen from the EDS analysis (Figure 5b inset) that AgNPs are present on the surfaces of the PA fibres. The EDS spectrum shows an intense peak corresponding to silver.

The remarkable increase in the number of dispersed AgNPs on the surface of plasma-treated PA fibres, in
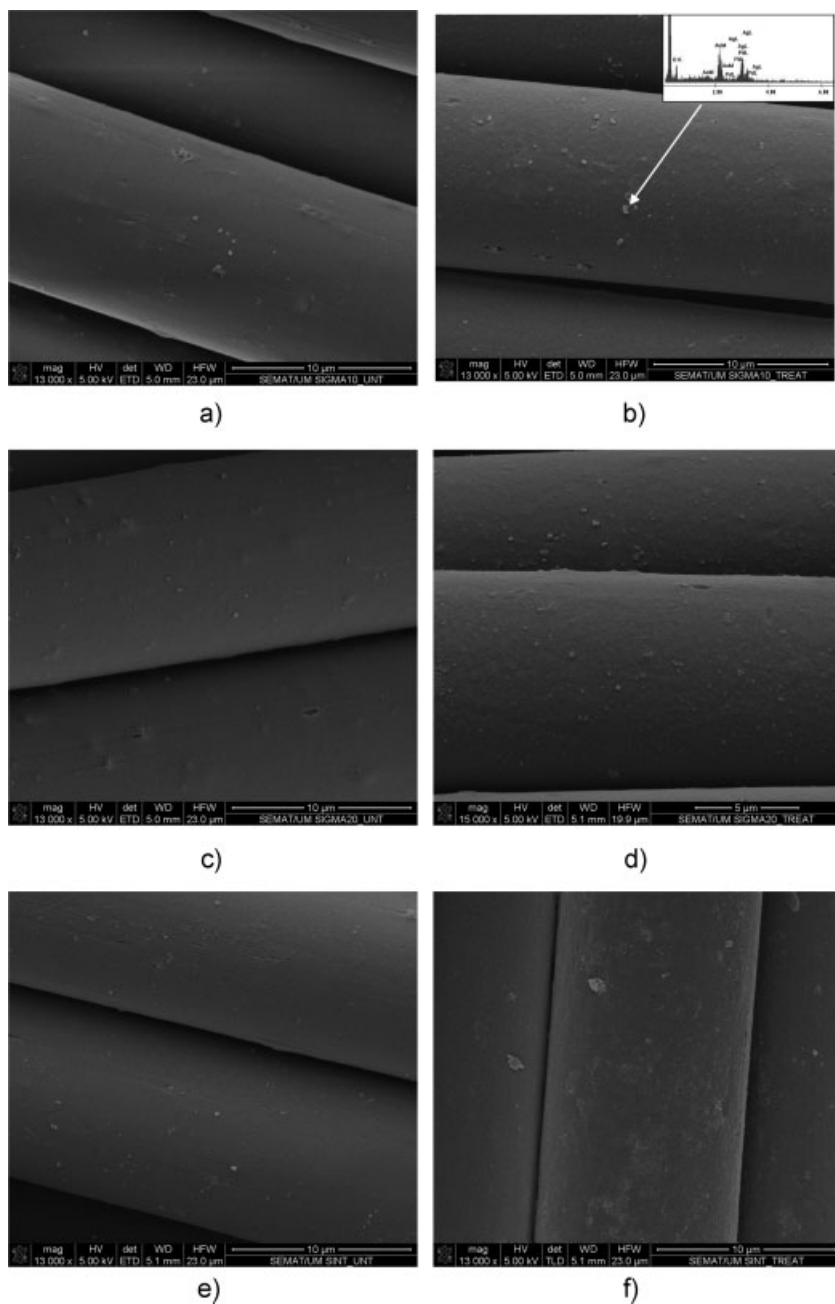
Figure 5. SEM images of PA fabrics loaded with AgNPs (20 ppm) with magnification of 13 000×: (a) Untreated PA with AgNPs Sigma10 (10 nm); (b) Plasma-treated PA with AgNPs Sigma10; (c) Untreated PA with AgNPs Sigma20 (20 nm); (d) Plasma-treated PA with AgNPs Sigma20; (e) Untreated PA with AgNPs synthetized (50 nm); (f) Plasma-treated PA with AgNPs Plasma-treated PA with AgNPs.

be necessary to get a complete clarification of the role of the NP size in the adsorption mechanism.

Figure 6 shows the XPS spectra of fibres surface in the region of binding energies associated to Ag $3d_{5/2}$ core-electrons confirming the presence of silver in the form of Ag^0.[61] All the binding energies are referenced to C1s (284.5 eV). Large differences between the peak intensities for silver nanoparticles determined before and after plasma treatment can be observed. Sigma 10 and 20 nm NPs loaded in plasma treated PA showed the more intense peaks in accordance with the higher loading values as confirmed by the reflectance spectroscopy. The observed binding energies of Ag $3d_{5/2}$ and Ag $3d_{3/2}$ are between 368 and 369 eV and between 374 and 375 eV, respectively. The energies are in good agreement with the literature values for the binding energies of silver nanoparticles.[62,63] However, the positive shift in binding energy of Ag $3d_{5/2}$ relative to the bulk Ag (368.3 eV) suggests that the silver nanoparticles are oxidized as a result of the interaction with the PA surface or that unreacted Ag^+ remains on the NPs surface.[64] Moreover, the observed shifts are proportional to the NPs size. The larger are the AgNPs, the higher are the binding energies.[64]

The influence of the loading of colloidal AgNPs onto PA fabric surface before and after plasma treatment was evaluated by measuring reflectance spectra. The homogeneous colour change obtained in the fabrics after AgNPs deposition is in accordance with literature data.[28] The colour changes were expressed as the increase in PA surface absorbance after AgNPs loading in both untreated and plasma treated fabrics, at the AgNPs maximum absorption wavelengths. According to the graphs in Figure 7 it can be explicitly seen that all the plasmatic treated samples gave a higher

diameter, otherwise it would also be noticed in the untreated fabric analysis. So, there seems to be a size-dependent effect on the AgNPs adsorption in the plasma treated PA fabrics. However, no definitive conclusions could be obtained. Further WDS and EDS analysis using different sized NPs at the same mass and number concentration will

absorption as compared with the untreated ones. The results obtained also confirm the higher AgNPs functionalization durability after washing on PA plasma-treated fibres using this loading method.[20,65] The decrease in specular reflection could be considered a direct measure of the Ag abundance in the topmost layer of the textile fabric.
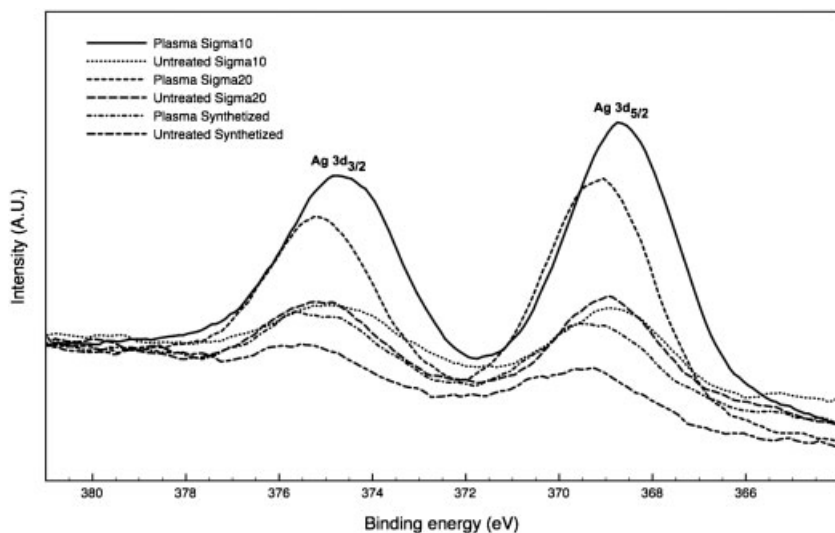
Figure 6. High-resolution XPS spectra of PA fibres surface in the binding energy region associated to Ag 3d5/2.
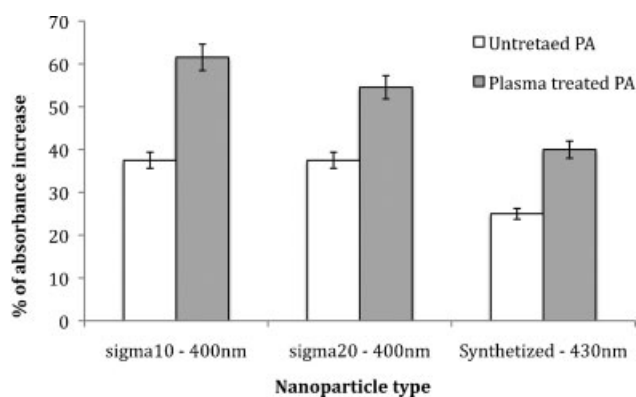

Figure 7. Percentage of increase in surface absorption at 400 (Sigma10 and 20) and 430 nm (synthetized) of untreated and plasma treated PA after silver nanoparticle deposition. Data are means ± SD ($n = 3$).

This means that there are more nanoparticles on the plasma treated samples than on the untreated ones. However, as previously discussed no definitive conclusion could be obtained for the synthetized nanoparticles due to their lower number and underestimated concentration. However, also in this case the significant differences between the 10 and 20 nm NPs in the plasma treated fabric when compared to the untreated fabrics seems to confirm a size-dependent effect.

Surface properties of the PA fabric were characterized by static and dynamic contact angle measurement based on the sessile drop principle. The static contact angle was measured in order to evaluate the wettability of PA fabrics after the application of AgNPs with and without plasma treatment. According to data attained in Table 4, all the

loaded AgNPs samples without plasma treatment possess slightly higher static contact angles as compared to the controls. This value can lead to a conclusion that the AgNPs reinforce the PA fabric hydrophobicity. In the plasma treated samples the drastic chemical changes of the plasma treatment confer high hydrophilicity and at the same time improve the NPs loading onto the fabric surface. The observed static contact angles in the plasma treated fabrics seem to be due to an equilibrium between the slight drop repulsive effect of the higher amount of AgNPs, that contrast the hydrophilic attraction of the plasma treated PA, and the protective effect of the NPs that seems to preserve the hydrophilicity by electrostatic interactions. Usually, with the increase in nanoparticle size, the specific surface area and free energy decrease, which should lead to an increase in the contact angle.[66,67] However, several other factors such as surface roughness, nanoparticle distribution and chemical interactions on the substrate, can also control the contact angle.[68]

The plasma treated control that was processed at the same conditions of the AgNPs loaded samples (cured at 100 °C and washed in citrate buffer without NPs) showed values of static angles similar to the untreated control. On the contrary the plasma-treated pristine control showed the lowest value of static contact angle. This is due to the non-permanent effect (aging) of the free radical and polar groups generation on the surface of plasma processed PA.[69] Increase in contact angle is usually observed after few days after plasma treatment.[15] Time, thermal and aqueous treatments and even the handling of the samples can degrade the effect generated by the plasma treatment according to the diffusion of the reactive species and the reorientation and folding under of the surface layers.[70]

Table 4. Static contact angle of the samples with and without plasma treatment.

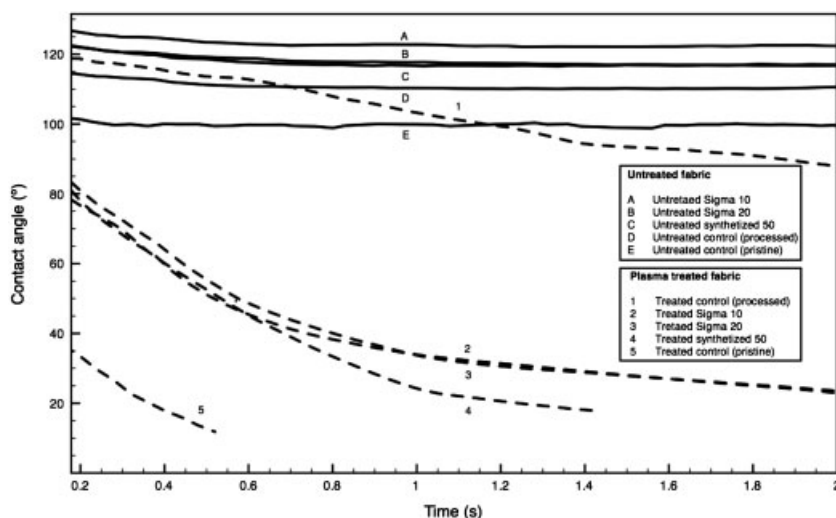| Sample	Untreated contact angle [°]	Plasma treated contact angle [°]
Control (pristine)	116.5 ± 1.0	59.3.4 ± 2.2
Controls (processed)	126.4 ± 6.1	125.7 ± 3.4
Sigma 10	131.2 ± 5.1	124.2 ± 2.8
Sigma 20	132.6 ± 6.9	115.0 ± 2.1
Synthetized	134.5 ± 4.4	94.7 ± 2.7

Data are means ± SD ($n = 3$).

Figure 8. Dynamic contact angle of the samples with and without plasma treatment. Straight lines: Untreated samples. Dotted lines: Plasma treated samples.

Despite the initial hydrophobic values of the static contact angles, the dynamic contact angle for all the plasma treated samples, with the exception of the processed control, show a dramatic contact angle reduction in <1 s, as all the untreated samples maintain hydrophobic contact angles (Figure 8). It seems that the AgNPs size and distribution alter the roughness and charge of the PA surface providing a slight increase in hydrophobicity. However, after the plasma treatment, this effect is completely annulled by the highly hydrophilic functional groups formed onto the PA surface. At the same time, the AgNPs electrostatic interactions with the new-formed functional groups appear to also have a protective effect on the plasma surface modifications. This can be noticed by the difference between the pristine (5) and the processed (1) controls. The effect of aging of plasma treatment is the highest in the processed control that without the protective effect of the AgNPs lost its initial hydrophilic properties showing values similar to the untreated samples. On the contrary, the plasma treated PA fabrics loaded with AgNPs preserve, in same extent, their hydrophilic properties (2, 3 and 4) especially the synthetized 50 nm NPs. The chemical reactivity of the AgNPs have shown a clear effect in decrease the surface energy of the PA surface stabilizing the chemical bonds that are generated by the plasma treatment. The biggest NPs, despite their lowest concentration, seem to favour higher electrostatic stabilization of the plasma-formed functional groups onto the PA surface. This is partially confirmed by the XPS analysis where a positive shift in binding energy of Ag relative to the bulk metal was observed. The shift is proportional to the NPs size. The larger are the AgNPs, the higher are the binding energies. This suggests that the bigger synthetized NPs have more Ag^+

ions on the NPs surface, probably due to the synthesis methodology that differ by the commercial NPs.[64]

4. Conclusion

The present research shows the effect on the deposition of three different size colloidal AgNPs onto DBD plasma pre-treated PA fabric. The two commercial (10 and 20 nm) NPs show monodisperse distribution, meanwhile the synthetized NPs (50 nm) show a larger polydispersity. All the NPs show good stability with no aggregation. The optimal energy dosage of DBD plasma discharge to modify the PA fabric surface properties was found at $2.5\,kW \cdot min \cdot m^{-2}$. The deconvolution analysis of C1s and O1s XPS peaks of the plasma treated PA confirms the decrease in the aliphatic functional groups and the remarkably increase of the oxygen singly bonded to carbon atoms. The SEM analysis indicates the well-dispersed deposition of the AgNPs on the PA fibres especially on the plasma pre-treated fabrics. The EDS, XPS and reflectance spectroscopy analysis confirm the presence of the Ag and seem to indicate in the 10 and 20 nm NPs a size-dependent adsorption. The smaller the diameter of AgNPs, the higher the amount of adsorbed NPs on the PA fibres. The estimation of the synthetized NPs concentration was difficult and probably underestimated because of the variation in particle number and the electrostatic effects on the plasma-treated textile. The DBD plasma treatment induces a threefold increase in Ag adsorption as compared with the untreated samples for all the NPs. The results of contact angle measurements showed a dual effect on the fabric wettability of the plasma treated fabric. AgNPs alters the roughness and charge of the PA surface providing hydrophobic properties and reducing the hydrophilicity of the plasma-treated PA surface. At the same time, the AgNPs appear to have a protective effect on the plasma surface modifications reducing the aging effect and maintaining high wettability. The 50 nm synthetized NPs seem to release a higher amount of Ag^+, as partially confirmed by the positive shift in binding energy, that provide higher electrostatic stabilizing effect on the plasma formed functional groups.

[1] T. Jeevani, *J. Nanomed. Nanotechnol.* **2011**, *2*, 124.

[2] R. Dastjerdi, M. Montazer, *Colloid Surf. B* **2010**, *79*, 5.

[3] C. H. Xue, S. T. Jia, J. Zhang, J. Z. Ma, *Sci. Technol. Adv. Mater.* **2010**, *11*, 1.

[4] I. P. Parkin, R. G. Palgrave, *J. Mater. Chem.* **2005**, *15*, 1689.

[5] S. Coyle, Y. Z. Wu, K. T. Lau, D. De Rossi, G. Wallace, D. Diamond, *MRS Bull.* **2007**, *32*, 434.

[6] A. P. S. Sawhney, B. Condon, K. V. Singh, S. S. Pang, G. Li, D. Hui, *Text. Res. J.* **2008**, *78*, 731.

[7] Y. Gao, R. Cranston, *Text. Res. J.* **2008**, *78*, 60.

[8] N. D. Oltargevskaya, G. E. Krichevsky, ''Textile finishing for the production of new generation medical textiles'', in *Medical Textiles and Biomaterials for Healthcare*, Eds., Woodhead Publishing Limited, Cambridge, UK **2006**, p. VIII/482.

[9] M. Rai, A. Yadav, A. Gade, *Biotechnol. Adv.* **2009**, *27*, 76.

[10] M. Ip, S. L. Lui, V. K. M. Poon, I. Lung, A. Burd, *J Med. Microbiol.* **2006**, *55*, 59.

[11] I. Chopra, *J. Antimicrob. Chemother.* **2007**, *59*, 587.

[12] H. Y. Lee, H. K. Park, Y. M. Lee, K. Kim, S. B. Park, *Chem. Commun.* **2007**, 2959.

[13] C. Damm, H. Munstedt, A. Rosch, *Mater. Chem. Phys.* **2008**, *108*, 61.

[14] M. S. Khalil-Abad, M. E. Yazdanshenas, M. R. Nateghi, *Cellulose* **2009**, *16*, 1147.

[15] G. Borcia, N. Dumitrascu, G. Popa, *Surf. Coat. Technol.* **2005**, *197*, 316.

[16] R. Morent, N. De Geyter, J. Verschuren, K. De Clerck, P. Kiekens, C. Leys, *Surf. Coat. Technol.* **2008**, *202*, 3427.

[17] F. R. Oliveira, A. P. Souto, N. Carneiro, J. H. O. Nascimento, *Mater. Sci. Forum.* **2010**, *636–637*, 846.

[18] C. X. Jia, P. Chen, W. Liu, B. Li, Q. A. Wang, *Appl. Surf. Sci.* **2011**, *257*, 4165.

[19] M. Gorensek, M. Gorjanc, V. Bukosek, J. Kovac, P. Jovancic, D. Mihailovic, *Text. Res. J.* **2010**, *80*, 253.

[20] M. Radetic, V. Ilic, V. Vodnik, S. Dimitrijevic, P. Jovancic, Z. Saponjic, J. M. Nedeljkovic, *Polym. Adv. Technol.* **2008**, *19*, 1816.

[21] V. Ilic, Z. Saponjic, V. Vodnik, S. Lazovic, S. Dimitrijevic, P. Jovancic, J. M. Nedeljkovic, M. Radetic, *Ind. Eng. Chem. Res.* **2010**, *49*, 7287.

[22] V. Ilic, Z. Saponjic, V. Vodnik, R. Molina, S. Dimitrijevic, P. Jovancic, J. Nedeljkovic, M. Radetic, *J. Mater. Sci.* **2009**, *44*, 3983.

[23] U. Kogelschatz, *Plasma Chem. Plasma Process.* **2003**, *23*, 1.

[24] G. Borcia, C. A. Anderson, N. M. D. Brown, *Surf. Coat. Technol.* **2006**, *201*, 3074.

[25] N. Y. Cui, D. J. Upadhyay, C. A. Anderson, N. M. D. Brown, *Surf. Coat. Technol.* **2005**, *192*, 94.

[26] L. Zhu, C. X. Wang, Y. P. Qiu, *Surf. Coat. Technol.* **2007**, *201*, 7453.

[27] T. Maneerung, S. Tokura, R. Rujiravanit, *Carbohydr. Polym.* **2008**, *72*, 43.

[28] V. Ilic, Z. Saponjic, V. Vodnik, B. Potkonjak, P. Jovancic, J. Nedeljkovic, M. Radetic, *Carbohydr. Polym.* **2009**, *78*, 564.

[29] L. F. Espinosa-Cristobal, G. A. Martinez-Castanon, R. E. Martinez-Martinez, J. P. Loyola-Rodriguez, N. Patino-Marin, J. F. Reyes-Macias, F. Ruiz, *Mater. Lett.* **2009**, *63*, 2603.

[30] J. R. Morones, J. L. Elechiguerra, A. Camacho, K. Holt, J. B. Kouri, J. T. Ramirez, M. J. Yacaman, *Nanotechnology* **2005**, *16*, 2346.

[31] H. L. Liu, S. A. Dai, K. Y. Fu, S. H. Hsu, *Int. J. Nanomed.* **2010**, *5*, 1017.

[32] P. C. Lee, D. Meisel, *J. Phys. Chem.* **1982**, *86*, 3391.

[33] S. Magdassi, A. Bassa, Y. Vinetsky, A. Kamyshny, *Chem. Mater.* **2003**, *15*, 2208.

[34] X. Y. Dong, X. H. Ji, H. L. Wu, L. L. Zhao, J. Li, W. S. Yang, *J. Phys. Chem. C* **2009**, *113*, 6573.

[35] A. Pyatenko, M. Yamaguchi, M. Suzuki, *J. Phys. Chem. C* **2007**, *111*, 7910.

[36] A. Henglein, M. Giersig, *J. Phys. Chem. B* **1999**, *103*, 9533.

[37] X. C. Jiang, W. M. Chen, C. Y. Chen, S. X. Xiong, A. B. Yu, *Nanoscale Res. Lett.* **2011**, *6*, 32.

[38] C. F. Li, D. X. Li, G. Q. Wan, J. Xu, W. G. Hou, *Nanoscale Res. Lett.* **2011**, *6*, 440.

[39] H. H. Huang, X. P. Ni, G. L. Loy, C. H. Chew, K. L. Tan, F. C. Loh, J. F. Deng, G. Q. Xu, *Langmuir* **1996**, *12*, 909.

[40] D. Fornasiero, F. Grieser, *J. Colloid Interface Sci.* **1991**, *141*, 168.

[41] O. Siiman, L. A. Bumm, R. Callaghan, C. G. Blatchford, M. Kerker, *J. Phys. Chem.* **1983**, *87*, 1014.

[42] S. M. Heard, F. Grieser, C. G. Barraclough, J. V. Sanders, *J. Colloid Interface Sci.* **1983**, *93*, 545.

[43] U. Kreibig, M. Quinten, D. Schoenauer, *Physica A* **1989**, *157*, 244.

[44] L. Rivas, S. Sanchez-Cortes, J. V. Garcia-Ramos, G. Morcillo, *Langmuir* **2001**, *17*, 574.

[45] R. M. Bright, M. D. Musick, M. J. Natan, *Langmuir* **1998**, *14*, 5695.

[46] C. H. Munro, W. E. Smith, M. Garner, J. Clarkson, P. C. White, *Langmuir* **1995**, *11*, 3712.

[47] P. V. Kamat, M. Flumiani, G. V. Hartland, *J. Phys. Chem. B* **1998**, *102*, 3123.

[48] Y. N. Xia, N. J. Halas, *MRS Bull.* **2005**, *30*, 338.

[49] R. A. Alvarez-Puebla, E. Arceo, P. J. G. Goulet, J. J. Garrido, R. F. Aroca, *J. Phys. Chem. B* **2005**, *109*, 3787.

[50] A. M. El Badawy, T. P. Luxton, R. G. Silva, K. G. Scheckel, M. T. Suidan, T. M. Tolaymat, *Environ. Sci. Technol.* **2010**, *44*, 1260.

[51] L. V. Stebounova, E. Guio, V. H. Grassian, *J. Nanopart. Res.* **2011**, *13*, 233.

[52] A. Sarkar, S. Kapoor, T. Mukherjee, *J. Phys. Chem. B* **2005**, *109*, 7698.

[53] M. Xi, Y. L. Li, S. Y. Shang, D. H. Li, Y. X. Yin, X. Y. Dai, *Surf. Coat. Technol.* **2008**, *202*, 6029.

[54] D. Pappas, A. Bujanda, J. D. Demaree, J. K. Hirvonen, W. Kosik, R. Jensen, S. McKnight, *Surf. Coat. Technol.* **2006**, *201*, 4384.

[55] Q. Zhou, K. A. Wang, L. S. Loo, *J. Mater. Sci.* **2011**, *46*, 3084.

[56] C. S. Ren, D. Z. Wang, Y. N. Wang, *J. Mater. Process. Technol.* **2008**, *206*, 216.

[57] F. R. Oliveira, L. Erkens, R. Fangueiro, A. P. Souto, *Plasma Chem. Plasma Process.* **2012**, *32*, 259.

[58] M. Montazer, A. Shamei, F. Alimohammadi, *Prog. Org. Coat.* **2012**, *74*, 270.

[59] M. M. Hossain, D. Hegemann, A. S. Herrmann, P. Chabrecek, *J. Appl. Polym. Sci.* **2006**, *102*, 1452.

[60] A. Hebeish, M. E. El-Naggar, M. M. G. Fouda, M. A. Ramadan, S. S. Al-Deyab, M. H. El-Rafie, *Carbohydr. Polym.* **2011**, *86*, 936.

[61] N. Bowering, D. Croston, P. G. Harrison, G. S. Walker, *Int. J. Photoenergy* **2007**, *90752*, 1.

[62] E. Stathatos, P. Lianos, P. Falaras, A. Siokou, *Langmuir* **2000**, *16*, 2398.

[63] R. Patakfalvi, A. Oszko, I. Dekany, *Colloids Surf. A* **2003**, *220*, 45.

[64] H. S. Shin, H. C. Choi, Y. Jung, S. B. Kim, H. J. Song, H. J. Shin, *Chem. Phys. Lett.* **2004**, *383*, 418.

[65] Z. Saponjic, V. Ilic, V. Vodnik, D. Mihailovic, P. Jovancic, J. Nedeljkovic, M. Radetic, *Pub. Astro. Obs. Belgr.* **2008**, *84*, 411.

[66] D. Chen, L. F. Tan, H. Y. Liu, J. Y. Hu, Y. Li, F. Q. Tang, *Langmuir* **2010**, *26*, 4675.

[67] A. M. Munshi, V. N. Singh, M. Kumar, J. P. Singh, *J. Appl. Phys.* **2008**, *103*, 1.

[68] X. M. Li, T. He, M. Crego-Calama, D. N. Reinhoudt, *Langmuir* **2008**, *24*, 8008.

[69] C. X. Wang, L. Zhu, Y. P. Qiu, *J. Appl. Polym. Sci.* **2008**, *107*, 1471.

[70] M. Kostic, N. Radic, B. M. Obradovic, S. Dimitrijevic, M. M. Kuraica, P. Skundric, *Plasma Process. Polym.* **2009**, *6*, 58.